Building a molecular-level picture of the ultrafast dynamics of the charge-transfer-to-solvent (CTTS) reaction of sodide (Na⁻)*

Ignacio B. Martini, Erik R. Barthel, and Benjamin J. Schwartz‡

Department of Chemistry and Biochemistry, University of California, Los Angeles, Los Angeles, CA 90095-1569, USA

Abstract: Charge-transfer-to-solvent (CTTS) reactions represent the simplest possible electron-transfer reaction. One of the reasons that such reactions have become the subject of recent interest is that transfer of a CTTS electron from an atomic anion to the solvent involves only electronic degrees of freedom, so that all the dynamics involved in the reaction are those of the solvent. Thus, CTTS reactions provide an outstanding spectroscopic window on the dynamics of the solvent during electron transfer. In this paper, we will review our recent work studying the CTTS reaction of the sodium anion, (Na⁻ or sodide) in a series of ether solvents. By comparing the results of ultrafast spectroscopic pump/probe experiments and mixed quantum/classical molecular dynamics simulations, we work to build a molecular-level picture of how solvent motions control the dynamics of CTTS, including the distance to which the electron is ejected and the rates of both the forward and back electron-transfer reactions.

INTRODUCTION

The photoionization of atoms and molecules in solution can take place at photon energies below that needed for direct photoejection of electrons into the conduction band of the solvent. This production of solvated electrons using low-energy excitation is known as charge-transfer-to-solvent, or CTTS [1–4]. The reason that below-threshold detachment can take place is that the polarization of the solvent molecules surrounding a solute creates a metastable, quasi-bound electronic state (the CTTS state) into which the most weakly bound solute electron can be photoexcited [5–9]. The transition between the highest-occupied molecular orbital of the solute and this solvent-supported CTTS excited state is usually strongly optically allowed, producing an intense CTTS absorption band that is absent in gas phase. Following excitation, the local solvent structure rearranges to accommodate both the quasi-bound excited electron and the ionized solute's new electronic structure, and it is this reorganization of the solvent that ultimately promotes detachment of the excited electron into a nearby cavity. The structure and dynamics of the solvent surrounding the solute not only control the detachment of the electron following CTTS excitation, but also control the fate of the solvated electron following ejection: for example, the rate of recombination is largely determined by the position where the detached electron is localized with respect to its geminate partner.

The fact that the solvent plays such a central role in CTTS, controlling both the forward (detachment) and backward (recombination) electron-transfer reactions, makes CTTS systems outstanding candidates for the molecular-level study of how solvent motions control the dynamics of electron transfer. In particular, for the case of monatomic solutes that have only electronic degrees of freedom, any

---

‡Corresponding author: E-mail: schwartz@chem.ucla.edu

spectroscopic changes observed during the course of a CTTS reaction must be a direct reflection of specific solvent motions in the vicinity of the donor solute. To this end, we have investigated the photophysics following CTTS electron detachment from sodium anions (Na⁻, or sodide) in a variety of ethers [10–12]. We chose to study this particular CTTS system for its spectroscopic convenience: All of the species in this reaction have well separated spectra and can be observed essentially independently. Figure 1 shows the absorption spectra of the ground-state sodide reactant, the CTTS excited-state (Na⁻*) intermediate, and the solvated electron and solvated sodium atom products in the solvent tetrahydrofuran, THF [10].

Over the past several years, our group has worked to understand the detailed dynamics of this reaction both experimentally [10–12] and theoretically [13]: this paper summarizes the salient results and reviews our latest thinking on this subject. In particular, we review our pump/probe transient absorption data for all the species whose absorption spectra are shown in Fig. 1. We will show how the experimental results suggest the formation of different kinds of electron:atom contact pairs following photodetachment, similar to the picture developed for the CTTS reaction of the aqueous halides [6]. We then test our picture by fitting the experimental results in different solvents to a multistep kinetic model that accounts for both the population dynamics and the effects of solvent relaxation on the ultrafast spectroscopy. By combining information from the pump/probe experiments with mixed quantum/classical molecular dynamics (MD) simulations, we speculate on the molecular details of the photoejection mechanism. We will argue that the rate-determining step in CTTS electron detachment from alkali metal anions is the solvent-induced migration of the node of the excited electronic wave function off of the parent alkali metal atom [13]. We then finish by constructing a plausible molecular-level picture of how local solvent motions determine all the dynamics of CTTS reactions.
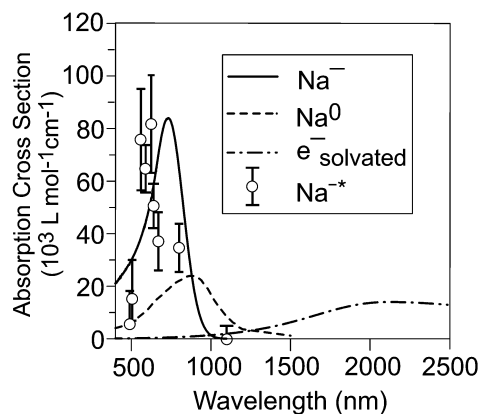
Fig. 1 Absorption spectra of all the species involved in the CTTS reaction of sodide in THF: Na⁻ (solid curve), Na⁻* (circles with 1σ error bars, determined from the DE+S model), Na⁰ (dashed curve), and the solvated electron (dashed–dotted curve).

EXPERIMENTAL AND COMPUTATIONAL METHODS

The details of the sodide synthesis and the photophysical experimental setup have been described previously [10–14]. Briefly, sodide solutions in THF were prepared by a modification of the technique originally described by Dye [15]. A similar procedure was used to prepare sodide solutions in tetrahydropyran (THP) and diethylether (DEE) [10]. The laser system used for the time-resolved experiments is a regeneratively amplified Ti:Sapphire laser [Spectra Physics] that produces ~120-fs pulses at 780 nm with a 1 kHz repetition rate. Visible and infrared laser pulses were produced by optical parametric amplification (OPA). All of the experiments were performed at room temperature. For all of the

data presented below, we found that the dynamics were independent of the relative polarization between the pump/probe pulses in THF, although significant polarization effects were observed in THP [10] (as well as in higher time resolution experiments in THF by Ruhman and coworkers) [16].

For the MD simulations of the Na⁻ CTTS process, we have used both a straight classical approach [17,18] as well as a mixed quantum/classical approach [13] in which only one of the sodide valence electrons was treated quantum mechanically, and the sodium nucleus and solvent molecules were treated classically. Since the Born–Oppenheimer approximation is not valid for the dynamics that take place during electron detachment, our mixed quantum/classical simulations use the electronically nonadiabatic mean-field-with-surface-hopping methodology (MF/SH) developed by Rossky and coworkers [19]. An extended discussion of both the application of this method to CTTS and the results presented below can be found in ref. [13].

RESULTS AND DISCUSSION

Building a molecular-level picture of the CTTS dynamics of Na⁻ in THF

The absorption of a visible photon by Na⁻ promotes one of the two sodide 3*s* valence electrons to a solvent-bound CTTS excited state, Na⁻*. Since the transition is strongly one-photon allowed, this suggests that the cavity-supported CTTS excited state is *p*-like in nature. The valence 3*s* electron is only loosely held by the Na nucleus (the electron affinity of Na is only ~0.5 eV [20]), making the ground-state sodium anion much larger than the ground state of a (neutral) sodium atom [20]. Since the solvent cannot move during the time the CTTS electron is promoted to the *p*-like solvent-supported excited state, the neutral sodium atom that remains after CTTS excitation is effectively isolated from the first-shell solvent molecules. In other words, CTTS excitation creates a transient gas-phase-like sodium atom that exists in an isolated environment until the closest solvent molecules have had time to translate inward and make contact. Thus, one of the spectroscopic signatures of CTTS excitation of Na⁻ should be a strong absorbance near 590 nm, reminiscent of the gas-phase Na D-line (cf. Fig. 1). This absorbance should then decrease as the solvent relaxes in response to the excitation, leading to both detachment of the electron and solvation of the initially isolated Na atom.

This type of behavior is indeed observed in Fig. 2, which shows the spectroscopic dynamics at a variety of probe wavelengths throughout the visible spectrum following CTTS excitation of Na⁻ in THF. In this figure (and those following), a positive differential absorption (or ΔOD) indicates the presence of a strongly absorptive species in that region of the spectrum, whereas a negative ΔOD represents
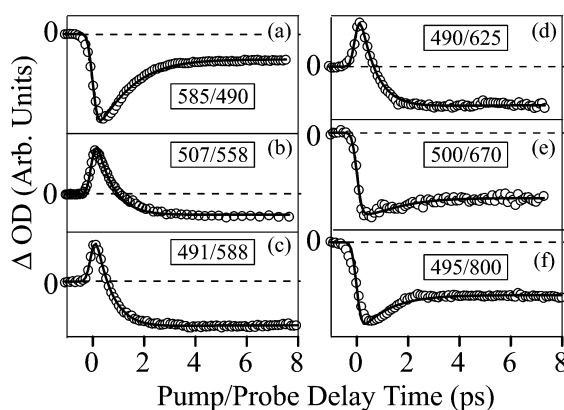

Fig. 2 Transient absorption dynamics of sodide in THF monitored for different pump/probe wavelength combinations throughout the visible. Positive signals correspond to excited-state absorption, while negative signals correspond to bleaching of the ground-state Na⁻. The solid lines are fits to the DE+S model; see text.

the expected bleach of the CTTS band due to the removal of a fraction of the Na$^-$ ground-state population. Clearly, for probe wavelengths in the vicinity of 590 nm (panels b–d), the intense transient absorption at early times confirms the presence of an electronic species that can be thought of as a sodium atom in a gas-phase-like environment. This absorption appears within the time resolution of our laser system (<200 fs) and does not decay for nearly a picosecond, providing a direct measure of the time it takes for the first-shell solvent molecules to move inward and solvate the Na core. Once this solvation process is complete, the pump/probe signals near 590 nm become negative. This bleach at times longer than a few ps, which is detected at all the visible wavelengths in Fig. 2, indicates that the CTTS-excited system does not relax directly back to the Na$^-$ ground state. Thus, CTTS excitation must have produced stable photoproducts, which can be no other than a solvated sodium atom and a solvated electron. Therefore, the decay of the 590-nm absorption signal in Fig. 2 must be directly related to the time for electron detachment from the CTTS excited state. A detailed kinetic modeling of the data in Fig. 2 (solid curves, details discussed further below) indicates that this decay takes ~800 fs in THF [10].

The fact that ejection of the electron following CTTS excitation is delayed in the Na$^-$/THF system stands in contrast to the results measured for the CTTS ionization of aqueous iodide, which is essentially instantaneous (<200 fs) [7]. We believe that the difference in dynamics between the CTTS reactions in halides and alkalides results from the fact that the electronic symmetry of these two systems are opposite: the sodide CTTS excited state has a *p*-like symmetry produced by excitation of an *s*-like ground state, whereas the iodide CTTS state has an *s*-like symmetry produced by excitation of an electron in a ground-state *p* orbital. To study the effects of the symmetry reversal on the photodetachment reaction, we performed nonadiabatic MD simulations on the CTTS excitation of Na$^-$ in water (even though the Na$^-$/water system cannot be prepared experimentally, we wanted to be able to directly compare to previous simulation work of the I$^-$ CTTS reaction [8,9] in this solvent). The results we obtained from a typical trajectory are summarized in Fig. 3 [13]. At a time delay of 10 fs, one of the sodide valence electrons is promoted into the CTTS excited state. The wave function of the excited electron clearly resides in the *p*-shaped particle-in-a-spherical-cavity state with the node centered at the atomic sodium core (20 fs). Solvation of the excited state starts almost immediately after its creation via translation of the closest solvent molecules into the orbital node. This translational relaxation continues until the solvent molecules encounter the sodium core, which prevents the positive end of the solvent dipoles from reaching the center of the node and providing the maximum possible stabilization of the bi-lobed negative charge distribution. This leaves the solvent with no choice but to rearrange in such a way as to cause the node to move off of the Na atom core. Indeed, by 750 fs, migration of the excited-state wave function has taken place so that one of the *p*-like lobes is pinned to the sodium atom core while the other lobe is extended into the solvent. This nodally migrated species exists for a relatively long time, until 1430 fs for this particular trajectory, when motions of the solvent finally induce the nonadiabatic transition of the electron into the ground state. This ground state no longer has a node (1440 fs), and in fact has no overlap between the wave function and the sodium atom: the nonadiabatic transition has led to the completion of CTTS electron detachment.

The CTTS detachment mechanism seen in Fig. 3 is indeed quite different from that seen for the aqueous halides, where once the lowest *s*-like CTTS state was reached, the excited electron could adiabatically detach, forming the ground state of an *s*-like hydrated electron [8,9]. Thus, the difference in symmetry between the halide and alkalide systems plays a direct role in their CTTS detachment dynamics: CTTS detachment is direct upon excitation of the halides, but a nonadiabatic transition appears to be required for CTTS detachment from the alkalides [13].

We note here that the detachment and solvation times for the trajectory in Fig. 3 do not precisely match the experimental results presented throughout this paper because the simulations used water as the solvent instead of THF. We believe, however, that the nodal migration mechanism is general to the sodide CTTS electronic structure, and does not depend on the choice of solvent. We note that our classical simulations in THF do show the same ~800 fs time scale for translational solvent relaxation that
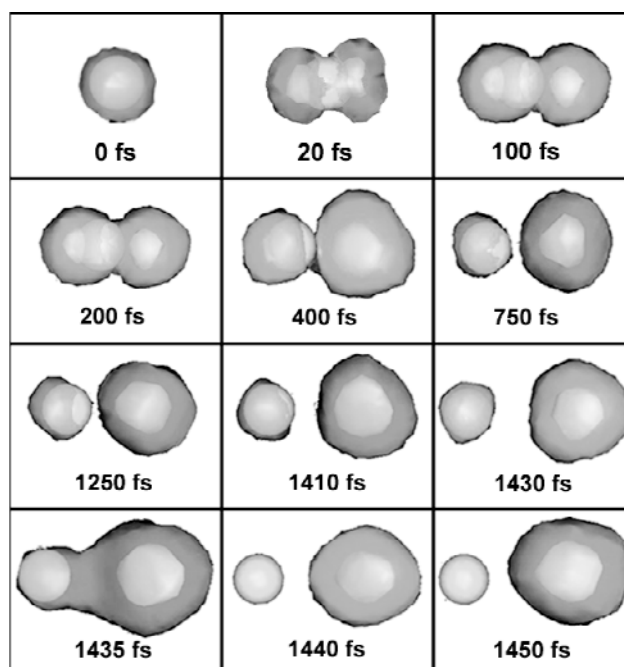
Fig. 3 Mixed quantum/classical nonadiabatic MD calculation [13] of the evolution of the excited-state electron density following CTTS excitation of Na$^-$ in water. The electron wave function is presented in two different shades of grey representing the 50 and 10 % charge density contours, respectively; while the spherical sodium core, shown in the lightest color, has the diameter of the Lennard–Jones Na–O σ parameter used in the calculations.

we observe in the experiments [18], and that mixed quantum/classical simulations in THF are presently under way [21].

The results from the MD simulations, together with the long-time bleach signals seen in Fig. 2, support the idea that detached solvated electrons are created after CTTS excitation. Although the bleach signals provide only indirect evidence that solvated electrons form following CTTS detachment, the presence of CTTS electrons can be monitored directly in the near IR region (cf. Fig. 1, which shows that the solvated electron in THF has its maximum absorbance near 2 μm) [22]. Figure 4 shows the results of pump/probe experiments monitoring the population of electrons as a function of the incident excitation wavelength, which reveal two distinctive features. First, the amplitude of the electron absorption signal at times longer than 2 ps is strongly dependent on the excitation energy, becoming larger at higher photon energies. Second, the decay of the electron's absorption, which we associate with the back electron-transfer reaction, takes place on three very different time scales: the signals decay in just a few ps (left panels of Fig. 4), relax on the hundreds of ps time scale (right panels of Fig. 4), and also persist for many ns (constant offset at times longer than 400 ps in the right panel of Fig. 4).

To rationalize these results, we have proposed that the freshly detached CTTS electrons can localize in one of three distinct spatial environments relative to their geminate sodium atom partners, as summarized schematically in Fig. 5. The localization position determines how quickly a detached electron can undergo recombination with its geminate sodium atom partner, leading to the three distinct time scales observed in the transient absorption signals [11]. The fraction of electrons that localize at each of the three distinct distances is in turn determined by the excitation wavelength. We will show below how this idea of distinct localization sites is supported by a kinetic scheme that not only explains the electron absorption decays presented in Fig. 4, but also the bleach recovery and 590-nm sodium
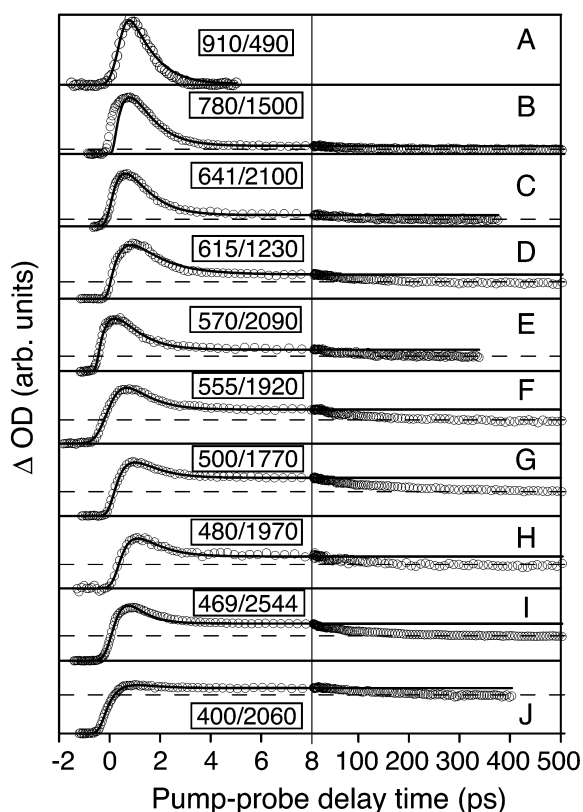
Fig. 4 Pump/probe scans monitoring the geminate recombination dynamics of the solvated electron after CTTS photodetachment. The left panel shows the short-time dynamics characteristic of the recombination of immediate contact pairs, while the right panel shows the long-time dynamics representing the recombination of the solvent-separated contact pairs. The solid curves in each of the left panels are fits to the DE+S model incorporating only the recombination of immediate pairs; these fits are also extrapolated onto the right panels, showing the fraction of longer-lived solvent-separated and free solvated electrons. The dashed lines in each panel correspond to the signal size remaining at times longer than 300 ps, and thus represent the fraction of free electrons. The difference in height between the solid and dashed curves at long times represents the fraction of electrons localized in solvent-separated contact pairs.

atom geminate-partner dynamics in Fig. 2, and similar data for the Na⁻ CTTS reaction in solvents other than THF.

At low excitation energies, the excited CTTS wave function is largely confined to the original solvent cavity containing the sodium atom, so that after ejection the electron lies in an *immediate contact pair*: the electron and the sodium atom share the same solvent cavity. Because the immediate-pair electron's wave function has significant overlap with its sodium atom partner, back electron transfer can take place quickly, in ~1 ps, as summarized on the left side of Fig. 5. At higher excitation energies, the electron is promoted into the continuum states in the conduction band of the liquid, allowing for direct ejection into the bulk of the solvent. If the continuum electron then localizes at a distance that is two or more solvent shells away from its parent sodium atom, we label it as a *free solvated electron*. Free solvated electrons do not undergo back electron transfer on sub-ns time scales, since their recombination is limited by diffusive encounters with their geminate Na^0 partners, nongeminate sodium atoms, or scavenging impurities [11]. Finally, the detached electron also can localize only one solvent shell away from the sodium atom, into what we define as a *solvent-separated contact pair*, depicted on the right side of Fig. 5. The back electron transfer of solvent-separated pairs cannot take place until an appro-
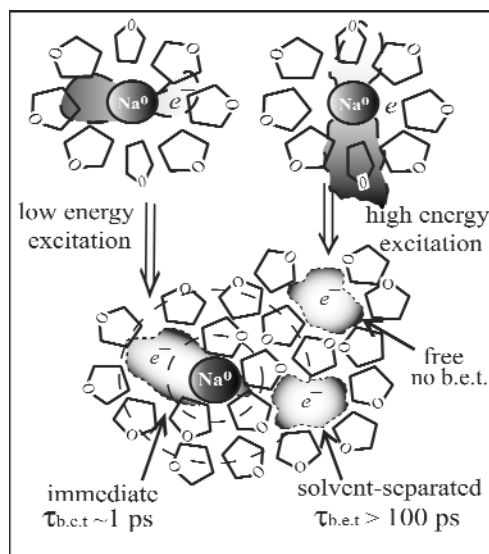
Fig. 5 Schematic representation of the photodetachment and localization of electrons following CTTS excitation of Na⁻ in THF. Low-energy excitation leads to immediate contact-pair formation, while higher-energy excitation can create either solvent-separated contact pairs or free electrons. See text for details.

priate fluctuation disrupts the local solvent structure and allows enough wave function overlap to drive the recombination reaction. Thus, solvent-separated contact pairs are metastable, and in THF at room temperature they do not recombine for hundreds of ps.

How do such metastable solvent-separated pairs form? We can imagine three different mechanisms via which CTTS excitation could produce solvent-separated contact pairs. First, as we have argued in previous work, photoexcitation of sodide to higher-lying bound CTTS states may be responsible for solvent-separated pair production. The idea is that these higher-lying states have a larger spatial extent that reaches into the second solvation shell, allowing for the possibility of detachment around an intervening solvent molecule (Fig. 5, top right) [11]. This picture, however, does not fit well with our mixed quantum/classical MD simulations, which suggest that nonadiabatic relaxation from either of the two higher-energy CTTS excited states to the lowest-energy CTTS excited state is very fast [13]. This leads to a second possibility for the production of solvent-separated contact pairs: that local heating of the first solvation shell allows the excited electron to escape to the second shell. The energy dissipated during nonadiabatic relaxation from one of the higher to the lowest CTTS state will be deposited in the vicinity of the first shell, providing a local heating that could significantly alter the detachment dynamics. We are presently working on temperature-dependent experiments to further explore this possibility. Finally, we cannot discard the possibility that solvent-separated contact pairs are created by direct ionization of sodide into the continuum, the same mechanism that produces free electrons. It is certainly possible that some fraction of the free electrons are produced close enough to their geminate partners to become trapped in solvent-separated pairs; thus, solvent-separated pairs may simply be another manifestation of excitation into the conduction band of the fluid.

Regardless of their formation mechanism, it is important to understand that solvent-separated contact-pair electrons exist as a distinct photoproduct of CTTS. For example, solvent-separated electrons not only show a distinct behavior in the fact that they undergo geminate recombination on a hundreds-of-picoseconds time scale (Fig. 4), but they also have a unique ability to undergo photo-induced geminate recombination. In a series of three-pulse experiments, we observed that excitation of the electrons in solvent-separated contact pairs resulted in an efficient recovery of the sodide population, whereas excitation of electrons in immediate contact pairs produced additional free electrons [12,24].

The different photophysical behaviors following reexcitation verify that immediate and solvent-separated contact-pair electrons do indeed comprise distinct photoproducts of the CTTS reaction.

To correlate the electron population distribution with excitation energy, we can compare the number of each distinct electron species—immediate contact pairs, solvent-separated contact pairs, and free electrons—by simply measuring the amplitude of the ~2-μm electron transient absorption decay on each of the distinct recombination time scales [23]. This analysis is presented in Fig. 6, which shows that the fraction of the signal corresponding to the number of solvent-separated contact pairs is very low, peaking at ~15 % for 500-nm excitation in THF and averaging less than 10 % over the entire CTTS absorption spectrum [23]. In contrast, immediate contact pairs are the dominant species at all excitation energies except at wavelengths shorter than ~450 nm, where free electrons predominate. This result emphasizes the idea that solvent-separated contact pairs are a relatively rare species created with low quantum yield, possibly because they are formed only through an indirect generation process, as discussed above.

Finally, we note that the electron-population distribution is not only determined by the *energy* of the laser excitation, but also by the *intensity* of the laser pulse. We have shown in previous work that sodide is a very effective two-photon absorber [11]. For example, at high excitation intensities at 800 nm, the resulting transient absorption signals behave as if they were a simple superposition of signals resulting from low-intensity 800-nm and 400-nm excitation. By looking at the fraction of the two-photon (400-nm) component of the signal, we were able to cleanly extract the two-photon cross-section of sodide at 800 nm [11,24].
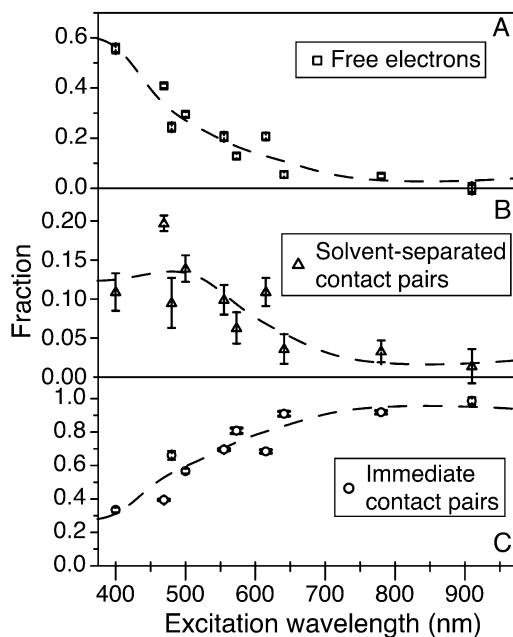
Fig. 6 Quantum yield of production of the different kinds of electrons following excitation into the CTTS band of sodide in THF. Panel (a) shows the quantum yield of free electrons, panel (b) the quantum yield of electrons in solvent-separated contact pairs, and panel (c) the quantum yield of immediate contact-pair electrons. These fractions were calculated from the DE+S model and the data shown in Fig. 4. The dashed curves are fits to a combination of Gaussian sub-bands that combine to reconstruct the sodide ground-state CTTS spectrum. Details of the fitting procedure are presented in ref. [23].

How the solvent controls the dynamics of the Na⁻ CTTS reaction

In order to gain further insight into our molecular picture of the Na⁻ CTTS reaction and the resulting population distribution of detached electrons, we have explored the dynamics of the sodide CTTS reaction in a variety of ether solvents. The circles in Fig. 7 show the CTTS dynamics of a selected set of pump/probe scans of Na⁻ in DEE (left panels) and THP (right panels). The data is qualitatively similar to the analogous scans in THF, but the specific rates for each step of the CTTS reaction are slightly different between the three solvents. For example, the recombination of immediate contact-pair electrons, represented by the initial decay of the electron's absorbance at IR probe wavelengths > 1500 nm, is completed by ~4 ps in THF (Fig. 4), but not for 6 ps in DEE (Fig. 7C) and 8 ps in THP (Fig. 7F). In contrast, the decay of the 590-nm absorbance, which we assigned to the disappearance of the sodium core due to electron detachment from the CTTS excited state, is similar in DEE (Fig. 7A) and THF (Fig. 2C) but takes ~50 % longer in THP (Fig. 7D). Further inspection of the data in Figs. 2, 4, and 7 reveals that all of the different characteristic CTTS reaction times scale differently in different solvents. Since the different reaction mechanisms are directly related to underlying motions of the solvent, the logical conclusion is that different specific solvent motions must be responsible for each aspect of the dynamics involved in the CTTS excitation of Na⁻.

One manifestation of the different solvent motions responsible for solvation of the initially prepared Na⁻* state and electron photodetachment can be seen in the transient absorption dynamics near 1200 nm, shown in panels B and E of Fig. 7. Unlike the data obtained probing the electron in the ~2-μm region, which show a delayed rise due to the time for electron detachment, the 1200-nm data in Figs. 7 B and E (and similar data taken in THF) [10,12] show an instrument-limited appearance. This instantaneous rise is followed by a very fast decay and then a subsequent slower rise whose ~800-fs time scale (in the case of THF) matches the absorption decay observed at 590 nm (and the rise at ~2 μm), followed by an additional decay on the few-ps time scale. Our interpretation is that the instrument-limited rise results from promotion of the *p*-like cavity-confined CTTS-excited electron to one of the higher *p*-like
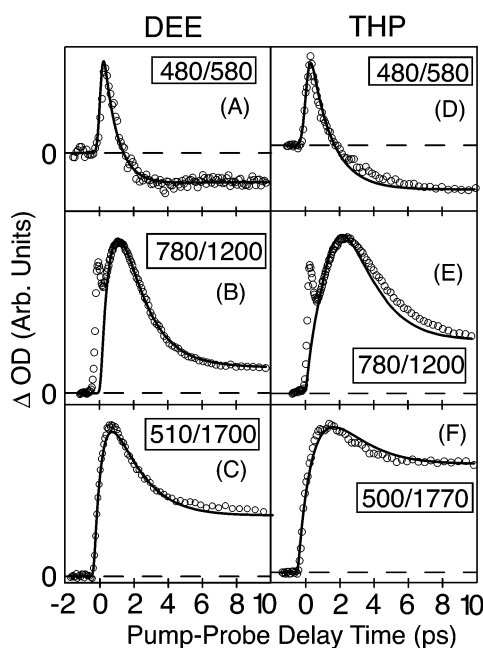
Fig. 7 Transient absorption dynamics of the CTTS reaction of sodide in DEE (left panels) and THP (right panels) at selected pump/probe wavelength combinations. Solid curves are fits to the DE+S model as explained in the text.

CTTS states. Although in principle this type of absorption should be forbidden by symmetry, the absorption is actually weakly allowed because the cavity is not perfectly spherical so that the electronic states do not have perfect p symmetry. This absorption then decays rapidly as solvent motions alter both the oscillator strength and the position of the energy levels involved in this p-like-to-p-like transition. The subsequent ~800-fs rise of the signal is due to the population growth of solvated electrons and solvated Na atoms due to detachment (since both absorb weakly at this wavelength, cf. Fig. 1), and the following decay reflects the loss of these species due to the recombination of immediate contact pairs (as is also observed in Figs. 2 and 4).

It is worth noting that the fast (~200-fs) decay of the 1200-nm signal in THF does not match the (~800-fs) decay of the 590-nm absorbing photoproduct, shown in Fig. 2, even though we assign both as being reflective of solvation processes affecting the CTTS excited state. This is because the 590-nm feature, which results from the D-line absorption of the Na atom core, is shielded from the solvent by the yet-to-be-detached excited electron. Thus, the earliest-time solvation processes that alter the absorption of the p-like electron do not affect the shielded core until after it is exposed by detachment of the excited electron. Overall, the fact that both the 1200-nm and 590-nm early-time absorption features appear universally across multiple solvents supports the idea that both are affiliated with the unsolvated CTTS excited state.
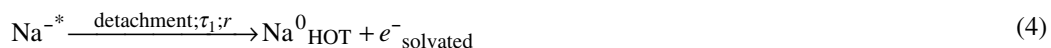
Detailed kinetic model for the Na⁻ CTTS reaction

To obtain a more quantitative understanding of how different solvent motions control the CTTS detachment and recombination of electrons from/to Na⁻, we have developed a kinetic model that accounts for what we believe are all of the distinct subprocesses involved in these reactions. The solid lines in Figs. 2, 4, and 7 represent a fit of the solvent-dependent data to what we refer to as "the delayed ejection plus solvation (DE+S) model", as introduced below. The details, assumptions, fitting procedure, and main results have been presented somewhere else [10,25]. The following kinetic equations define the DE+S model:

Photoexcitation:

$$\text{Na}^- \xrightarrow{\;h\nu\;} \text{Na}^{-*} \tag{1}$$

CTTS detachment:

$$\text{Na}^{-*} \xrightarrow{\;\text{CTTS};\tau_1;p\;} (\text{Na}^0{}_\text{HOT} \bullet e^-{}_\text{solvated})_\text{im} \tag{2}$$

$$\text{Na}^{-*} \xrightarrow{\;\text{CTTS};\tau_1;q\;} (\text{Na}^0{}_\text{HOT} \bullet e^-{}_\text{solvated})_\text{sep} \tag{3}$$

$$\text{Na}^{-*} \xrightarrow{\;\text{detachment};\tau_1;r\;} \text{Na}^0{}_\text{HOT} + e^-{}_\text{solvated} \tag{4}$$

Solvation dynamics:

$$[\text{Na}^0]^\text{total}_\text{HOT} \xrightarrow{\;\text{solvation};S(t_1,t_2)\;} [\text{Na}^0]^\text{total}_\text{equilibrium} \tag{5}$$

Back electron transfer (recombination) of contact pairs:

$$(\text{Na}^0 \bullet e^-{}_\text{solvated})_\text{im} \xrightarrow{\;\text{recombination};\tau_2\;} \text{Na}^- \tag{6}$$

$$(\text{Na}^0 \bullet e^-{}_\text{solvated})_\text{sep} \xrightarrow{\;\text{recombination};\tau_3\;} \text{Na}^- \tag{7}$$

Dissociation of contact pairs and diffusive recombination:

$$(Na^0 \bullet e^-_{solvated})_{sep} \xrightarrow{\text{dissociation};\tau_4} Na^0 + e^-_{solvated} \qquad (8)$$

$$Na^0 + e^-_{solvated} \xrightarrow{\text{diffusion};\tau(E)} Na^- \qquad (9)$$
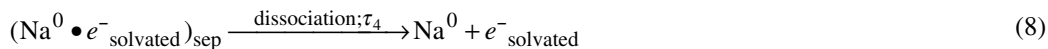
For the short-time dynamics ($t < 10$ ps) described by eqs. 1–6, the relevant kinetic parameters are τ_1 (the CTTS electron detachment time), τ_2 (the time for recombination of immediate contact pairs), and p (the fraction of electrons ejected into immediate contact pairs). The photophysical parameters ε_{Na^-}, ε_{Na^-*}, ε_{e^-}, t_1, t_2, and $\varepsilon_{Na}(\omega, t)$ correspond to the absorption cross-sections of sodide, the CTTS excited state, and the solvated electron, the times over which the Na^0 spectrum changes due to solvation, and the instantaneous Na^0 absorption spectrum at time t, respectively. The DE+S model uses static absorption spectra for the Na^-* CTTS excited state, the solvated electron, and the bleach of Na^-. In contrast, the Na^0 spectrum is allowed to shift and broaden due to solvation dynamics. A summary of the estimated parameters obtained through this fitting procedure (we note that there was an error in the table originally presented in ref. [10]) is shown in Table 1 [26]:

Table 1 Estimated model parameters with 95 % confidence interval.

Solvent	τ_1[a]	τ_2[a]	t_1[a]	t_2[a]
THF	0.84 ± 0.07	0.59 ± 0.10	1.12 ± 0.23	1 ± 1
THP	1.73 ± 0.08	0.69 ± 0.04	1.2 ± 0.99	2.2 ± 1.5
DEE	1.1 ± 1.0	1.2 ± 1.0	1.61 ± 0.50	2.1 ± 2.4

[a]These times, in picoseconds, are the forward and reverse electron transfer times (τ_1 and τ_2, respectively) for the Na^- CTTS reaction, and the solvation times for the wavelength maximum (t_1) and spectral width and oscillator strength (t_2) of the shifting Na^0 spectrum; see ref. [10] for details.

Close examination of eqs. 1–6 reveals that the initial fast decay of the absorption signal in the 1200–1500 nm wavelength range (Figs. 7 B and E) is not accounted for in the kinetic model. Thus, when fitting the model in this wavelength range, the data points between –1 and ~0.5 ps were excluded from the analysis. The fitting parameters in Table 1 for the CTTS dynamics in all three solvents show that the forward electron-transfer times (τ_1) increase in the order THF, DEE, and THP but that the back electron-transfer (geminate recombination) times for immediate contact pairs (τ_2) increase in the order THF, THP, DEE, in order of decreasing polarity. It is clear, then, that different solvent motions are responsible for the different underlying steps of CTTS reactions. The question that remains to be answered is what solvent characteristics can explain the different trends presented in Table 1.

The MD simulation results in Fig. 3 suggest that it is the ability of a few first-shell solvent molecules to translate into the node of the CTTS-excited wave function that limits the rate of CTTS detachment (τ_1) [13]. THF, which presents the fastest detachment time, is a nearly planar, disk-like molecule. The classical MD simulations of liquid THF molecule performed in our group [18] suggest that the translational and rotational motions of the first-shell THF molecules are coupled, and that this coupled motion is the most likely candidate to promote detachment and create the solvent cavity into which the electron localizes upon ejection [17]. DEE, on the other hand, is an open molecule that can freely rotate around its C–O bonds. These rotations cause DEE to have a more disordered solvent structure than THF, so that it takes longer for solvent translations to respond to CTTS excitation. Finally, THP is very similar in structure to cyclohexane. We speculate that THP will form "chair-like" structures that stack well in the liquid phase [27], thus, significantly reducing the ability of the first-shell solvent mol-

ecules to translate because they must first unstack before they can move into the nodal region of the excited CTTS wave function.

Table 1 also shows that the back electron-transfer times for immediate contact pairs (τ_2 in the DE+S model) decrease with increasing solvent polarity. We believe that this trend is due to the fact that the size of the solvated electron is inversely proportional to the solvent polarity: The more polar the solvent, the more localized the electron, and therefore, the higher the average electronic density. Barbara and coworkers have shown that the probability for a solvated electron to react with a nearby scavenger is proportional to the electron density in contact with that scavenger [28,29]. In other words, it is the overlap between the solvated electron's wave function with the vacant 3s orbital on the sodium atom that should determine the rate of immediate-pair back electron transfer. Because electrons are more localized in THF, the most polar solvent, they should have the greatest wave function overlap with the nearby sodium atom, leading to the highest back electron-transfer rate (lowest recombination time τ_2).

In addition to the decay of immediate contact pairs, the DE+S model can also account for the recombination of solvent-separated contact-pair electrons, eqs. 7–9. However, it is difficult to quantitatively extract parameters about the solvent-separated contact-pair recombination for several reasons. First, the disappearance of solvent-separated contact pairs does not follow either simple exponential behavior or a physically reasonable diffusion rate law [11]. Bradforth and coworkers have noted that the recombination of such species should be better modeled as diffusion over a potential barrier [6], but since we have no idea of what the size and shape of the barrier should be, including this type of behavior in the DE+S model is problematic. Second, the small relative amount of solvent-separated species (<15 % for all excitation wavelengths, cf. Fig. 6) [23] makes the determination of rate constants subject to large intrinsic errors. Third, we have no clear way to account for solvent-separated pairs that dissociate into free electrons before recombining, or to account for free electrons that become trapped into solvent-separated pairs during the first few hundred ps. Therefore, we offer only a qualitative discussion of the nature of the long-time back electron transfer.

Figure 8 shows the long-time CTTS dynamics of sodide in each of the three ether solvents. To better compare the dynamics (given that the fraction of electrons that localize into solvent-separated contact pairs differs between solvents even at the same excitation wavelength), the signals in Fig. 8 were normalized to the same value at 8 ps. The figure makes it clear that the long-time relaxation in DEE following excitation at ~490 nm is much faster than in THF or THP, and that in these two solvents the electron presents similar long-time decay kinetics. We speculate that solvent polarity plays an important role in the explanation of these observations. In DEE, the low polarity of this solvent causes the sol-
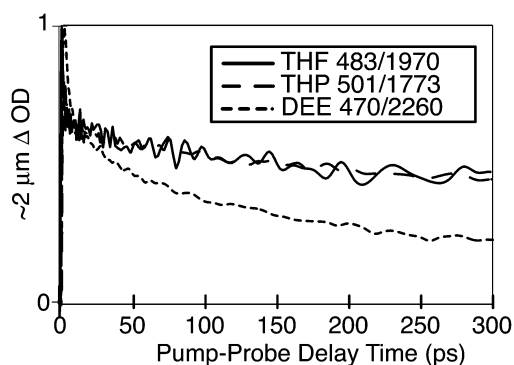
Fig. 8 Long time decay of the ~2-μm absorption of the solvated electron after CTTS excitation of Na$^-$, showing the geminate recombination of solvent-separated contact pairs in THF (solid curve), THP (dashed curve), and DEE (dotted curve). The data are scaled to the same value at 8 ps (after the immediate contact pairs have completed their geminate recombination) for ease of comparison.

vated electron to be significantly delocalized. Therefore, the electronic wave function can easily circumvent the one solvent molecule that obstructs the overlap with the parent sodium atom and promote recombination. As the solvent polarity increases, it provides progressively more stabilization for the solvent-separated contact pairs, so that the electron becomes more localized in the solvent-separated cavity and the barrier for recombination gets higher. In the language of Marcus theory, we would argue that the back electron transfer of solvent-separated pairs lies in the inverted regime: increasing the polarity of the solvent stabilizes the Na^- back electron transfer product and thus increases the driving force, but also increases the height of the barrier that must be overcome for recombination to take place [30]. This argument suggests that the barrier for back electron transfer is similar for the two cyclic ethers. It is likely that other microscopic details of the solvent structure surrounding the electron and the sodium geminate partner, such as the size and conformation of the solvent molecules, are involved in the electron recombination dynamics, as we will explore in our upcoming MD simulations of the CTTS process in nonaqueous solvents [21].

CONCLUSIONS

The study of the sodide CTTS system provides detailed information about how solvent motions and liquid structure determine the rates of electron-transfer reactions. By performing experiments in different solvents, we found that the rate at which an electron is ejected into solution depends on the local solvent structure and dynamics around the parent anion. More specifically, our MD simulations suggested that translational motions of the first-shell solvent molecules bear the primary responsibility for CTTS detachment. On the other hand, the back electron transfer that regenerates Na^- depends more on static solvent characteristics that determine the barrier for this reaction. For example, higher solvent polarity results in more localized electron wave functions, which results in a better overlap with the $3s$ orbital of the geminate Na^0 partners and therefore in a faster recombination of immediate pairs. In contrast, solvated electrons in solvent-separated contact pairs have increasingly stable solvation structures and move farther into the Marcus inverted regime in more polar solvents. A combination of polarity, local solvent conformation, and molecular size controls the survival time of the solvent-separated contact pair. In summary, each process in the CTTS reaction depends on the solvent in a different way.

ACKNOWLEDGMENTS

REFERENCES

1. L. Lehr, M. T. Zanni, C. Frischkorn, R. Weinkauf, D. M. Neumark. *Science* **284**, 635 (1999); A. V. Davis, M. T. Zanni, C. Frischkorn, D. M. Neumark. *J. Electron Spectrosc. Relat. Phenom.* **108**, 203 (2000); M. T. Zanni, C. Frischkorn, A. V. Davis, D. M. Neumark. *J. Phys. Chem. A* **104**, 2527 (2000); A. V. Davis, M. T. Zanni, R. Weinkauf, D. M. Neumark. *Chem. Phys. Lett.* **353**, 455 (2002).
2. F. H. Long, X. Shi, H. Lu, K. B. Eisenthal. *J. Phys. Chem.* **98**, 7252 (1994); F. H. Long, H. Lu, X. Shi, K. B. Eisenthal. *Chem. Phys. Lett.* **169**, 165 (1990); F. H. Long, H. Lu, K. B. Eisenthal. *J. Chem. Phys.* **91**, 4413 (1989).
3. Y. Gauduel, M. Sander, H. Gelabert. *J. Mol. Liq.* **78**, 111 (1998); H. Gelabert and Y. Gauduel. *J. Phys. Chem.* **100**, 13993 (1996); Y. Gauduel, H. Gelabert, M. Ashokkumar. *Chem. Phys.* **197**, 167 (1995); Y. Gauduel, H. Gelabert, M. Ashokkumar. *J. Mol. Liq.* **64**, 57 (1995).

4. See, e.g., F. H. Long, H. Lu, X. Shi, K. B. Eisenthal. *Chem. Phys. Lett*. **185**, 47 (1991); S. Pommeret, A. Antonetti, Y. Gauduel. *J. Am. Chem. Soc*. **113**, 9105 (1991); R. Laenen, T. Roth, A. Laubereau. *Phys. Rev. Lett.* **85**, 50 (2000); A. Hertwig, H. Hippler, A. N. Unterreiner, P. Vöhringer. *Ber. Bunsenges. Phys. Chem.* **102**, 805 (1998); J. L. McGowen, H. M. Ajo, J. Z. Zhang, B. J. Schwartz. *Chem. Phys. Lett*. **231**, 504 (1994); C. L. Thomsen, D. Madsen, S. R. Keiding, J. Thøgersen. *J. Chem. Phys*. **110**, 3453 (1999); C. Pepin, D. Houde, H. Remita, T. Goulet, J.-P. Jay-Gerin. *J. Phys. Chem. A* **101**, 4351 (1997); M. U. Sander, U. Brummund, K. Luther, J. Troe. *J. Phys. Chem.* **97**, 8378 (1993); Y. Hirata and N. Mataga. *J. Phys. Chem*. **95**, 1640 (1991); D. M. Bartels and R. A. Crowell. *J. Chem. Phys. A* **104**, 3349 (2000).
5. H. Y. Chen and W.-S. Sheu. *J. Am. Chem. Soc*. **122**, 7534 (2000); H. Y. Chen and W.-S. Sheu. *Chem. Phys. Lett*. **335**, 475 (2001); H. Y. Chen and W.-S. Sheu. *Chem. Phys. Lett*. **353**, 459 (2002).
6. S. E. Bradforth and P. Jungwirth. *J. Phys. Chem. A* **106**, 1286 (2002).
7. V. H. Vilchiz, J. A. Kloepfer, A. C. Germaine, V. A. Lenchenkov, S. E. Bradforth. *J. Phys. Chem. A* **105**, 1711 (2001); J. A. Kloepfer, V. H. Vilchiz, V. A. Lenchenkov, A. C. Germaine, S. E. Bradforth. *J. Chem. Phys*. **113**, 6288 (2000); J. A. Kloepfer, V. H. Vilchiz, V. A. Lenchenkov, S. E. Bradforth. *Chem. Phys. Lett*. **298**, 120 (1998).
8. W.-S. Sheu and P. J. Rossky. *J. Phys. Chem*. **100**, 1295 (1996); W.-S. Sheu and P. J. Rossky. *J. Am. Chem. Soc*. **115**, 7729 (1993); W.-S. Sheu and P. J. Rossky. *Chem. Phys. Lett*. **213**, 233 (1993); W.-S. Sheu and P. J. Rossky. *Chem. Phys. Lett*. **202**, 186 (1993).
9. A. Staib and D. Borgis. *J. Chem. Phys*. **103**, 2642 (1995); A. Staib and D. Borgis. *J. Chem. Phys*. **104**, 9027 (1996); A. Staib and D. Borgis. *J. Chem. Phys*. **104**, 4776 (1996).
10. E. R. Barthel, I. B. Martini, E. Keszei, B. J. Schwartz. *J. Chem. Phys*. **118**, 5916 (2003).
11. I. B. Martini, E. R. Barthel, B. J. Schwartz. *J. Chem. Phys*. **113**, 11245 (2000); E. R. Barthel, I. B. Martini, B. J. Schwartz. *J. Chem. Phys*. **112**, 9433 (2000).
12. I. B. Martini, E. R. Barthel, B. J. Schwartz. *J. Am. Chem. Soc*. **124**, 7622 (2002); I. B. Martini, E. R. Barthel, B. J. Schwartz. *Science* **293**, 462 (2001).
13. C. J. Smallwood, W. B. Bosma, R. E. Larsen, B. J. Schwartz. *J. Chem. Phys*. **119**, 11263 (2003).
14. T.-Q. Nguyen, I. B. Martini, J. Liu, B. J. Schwartz. *J. Phys. Chem. B* **104**, 237 (2000).
15. J. L. Dye. *J. Phys. Chem*. **84**, 1084 (1980); J. L. Dye. *J. Chem. Ed*. **54**, 332 (1977); M. T. Lok, F. J. Tehan, J. L. Dye. *J. Phys. Chem*. **76**, 2975 (1972).
16. Z. Wang, O. Shoshana, B. Hou, S. Ruhman. *J. Phys. Chem. A* **107**, 3009 (2003).
17. D. Aherne, V. Tran, B. J. Schwartz. *J. Phys. Chem. B* **104**, 5382 (2000); V. Tran and B. J. Schwartz. *J. Phys. Chem. B* **103**, 5570 (1999).
18. M. J. Bedard-Hearn, R. E. Larsen, B. J. Schwartz. *J. Phys. Chem. A* **107**, 4773 (2003); M. J. Bedard-Hearn, R. E. Larsen, B. J. Schwartz. *J. Phys. Chem. B* **107**, 14464 (2003).
19. K. F. Wong and P. J. Rossky. *J. Phys. Chem. A* **105**, 2546 (2001); *J. Chem. Phys*. **116**, 8418 (2002); **116**, 8429 (2002).
20. C.-N. Liu and A. F. Strance. *Phys. Rev. A* **59**, 3643 (1999).
21. M. J. Bedard-Hearn, C. J. Smallwood, R. E. Larsen, B. J. Schwartz. (2004). Manuscript in preparation.
22. L. M. Dorfman, F. Y. Jou, R. Wageman. *Ber. Bunsenges. Phys. Chem.* **75**, 681 (1971); F. Y. Jou and L. M. Dorfman. *J. Chem. Phys*. **58**, 4715 (1973); F. Y. Jou and G. R. Freeman. *Can. J. Chem.* **54**, 3693 (1973).
23. E. R. Barthel and B. J. Schwartz. *Chem. Phys. Lett*. **375**, 435 (2003).
24. I. B. Martini and B. J. Schwartz. *Chem. Phys. Lett*. **360**, 22 (2002).
25. L. Turi, P. Holpár, E. Keszei. *J. Phys. Chem. A* **101**, 5469 (1997); E. Keszei, T. H. Murphrey, P. J. Rossky. *J. Chem. Phys*. **99**, 22 (1995).

26. The complete global fit of the data to the DE+S model includes 21 pump/probe scans each in THF, DEE, and THP, which gives an average of ≤1.5 adjustable parameters for each pump/probe scan. These are substantially fewer adjustable parameters than would have resulted from simple bi-exponential fits to each scan (see ref. [10] for details).

27. J. G. Harris and F. H. Stillinger. *J. Chem. Phys*. **95**, 5953 (1991).

28. P. Kambhampati, D. H. Son, T. W. Kee, P. F. Barbara. *J. Phys. Chem. A* **106**, 2374 (2002); T. W. Kee, D. H. Son, P. Kambhampati, P. F. Barbara. *J. Phys. Chem. A* **105**, 8434 (2001); D. H. Son, P. Kambhampati, T. W. Kee, P. F. Barbara. *J. Phys. Chem. A* **105**, 8269 (2001).

29. This idea is also consistent with our work showing control over the back electron transfer of Na^0:solvated-electron contact pairs by changing the electron density of the solvated electron using a sequence of femtosecond laser pulses; see ref. [12].

30. Kohler and coworkers have seen a similar result for the recombination of hydrated electrons with aqueous indole radical cation, see: J. Peon, G. C. Hess, J. M. L. Pecourt, T. Yuzawa, B. Kohler. *J. Phys. Chem. A* **103**, 2460 (1999).